LUDWIG-MAXIMILIANS-UNIVERSITÄT
MÜNCHEN

BACHELOR THESIS

Aharonov-Bohm effect in helical systems

Florian Stäbler

supervised by
Prof. Dr. Jan von Delft
and
Dr. Oleg Yevtushenko

28th June 2017

LUDWIG-MAXIMILIANS-UNIVERSITÄT
MÜNCHEN

BACHELOR ARBEIT

Aharonov-Bohm Effekt in helikalen Systemen

Florian Stäbler

28. Juni 2017

Contents

Abstract

Helical states are a special state of matter with a lock-in relation between momentum and spin of electrons or quasi particle excitations. It has recently been shown, that many body effects can lead to the formation of helical edge states in one dimensional quantum wires. This results in highly interesting transport properties, like the ideal transport of charge and spin, for future electronic devices [1–5]. However, there is no direct experimental evidence confirming the helical transport in 1D. Therefore, it is highly important to develop new theoretical suggestions, which could help to find smoking gun evidence of helical states in 1D wires. In this work we have investigated the Aharonov-Bohm (AB) effect in helical systems as a tool to detect the helical nature in 1D wires. We have considered two possible setups, a helical AB-ring connected to helical leads and a helical AB-ring connected to metallic non-helical leads, and have shown, that the latter setup yields oscillations under certain conditions, whereas they are absent in the full helical setup. We believe our results can be used as a hint to develop reliable tools and thus proof helical transport in 1D quantum wires.

1 Introduction

1.1 The road to helical edge states

Our everyday experience shows that matter appears in different phases. In 1937, Lev Landau suggested a principle which characterizes states in terms of symmetries that are spontaneously broken. This allows to distinguish different phases of matter with local order parameters, a local measurement reveals whether a symmetry is broken or not. [6]

Klaus von Klitzing discovered the quantum hall effect (QHE) in the early 1980s, which illuminated a new aspect of phases of matter. He placed a two dimensional electron gas (2DEG) in a strong magnetic field at very low temperatures. [7] The quantization of the electron's orbital motion perpendicular to the magnetic field with the cyclotron frequency ω_c leads to the existence of quantized Landau levels with energy $E_m = \hbar\omega_c(m + 1/2)$. If N Landau levels are occupied and the rest are empty, then an energy gap separates the occupied and empty states just like in an insulator. A skipping motion of the edge's electron's orbit leads to the formation of one dimensional transport channels with a quantized conductance of e^2/h per channel. Unlike an insulator, an external electric field causes the cyclotron orbits to drift leading to a (transverse) Hall current characterized by the quantized Hall conductivity

$$\sigma_{xy} = Ne^2/h. \tag{1}$$

This very exact quantization could be explained by a fundamentally different approach to classify states which involves the concept of topology. The state responsible for the QHE does not break any underlying symmetries, except for time reversal symmetry (TRS) but it defines a topological phase in the sense, that smooth changes in the materials parameter do not effect the quantized value of the Hall conductance. It is reflected by the possibility to be characterized by a topological invariant, which can only take integer multiples of e^2/h. In mathematics the concept of topology defines different equivalence classes of shapes, which only differ by a smooth deformation of the shapes, especially without creating a hole in the deformation process, or ripping the object apart, or glueing it. In condensed matter physics one can consider a general crystal Hamiltonian $H(\mathbf{k})$ with an energy gap separating the valence and the conduction band. All Hamiltonians, which only differ by a smooth transformation of its parameters, which does not close the gap, can be seen as members of the same topological class. They belong to the same topological equivalence class characterized by a topological invariant n.

This invariant is referred to as the Chern number or TKNN number [8]. The Chern number can be understood physically in terms of the Berry phase. A closed path in k-space contributes as an extra phase to the electrons wave function as a line integral of $A_m = i \langle u_m | \nabla_k | u_m \rangle$, where u_m stand for the Bloch wave functions. It can also be expressed as a surface integral of the Berry flux. The Chern invariant can be expressed as integral over the Berry flux in one Brioullin zone.

$$n_m = \frac{1}{2\pi} \int d\mathbf{k}^2 F_m \quad F_m = \nabla \times A_m. \tag{2}$$

The total Chern number summed over all occupied bands $n = \sum_{m=1}^{N} n_m$ is a topological invariant in the sense that it can not change when the Hamiltonian varies smoothly.

Every QH state with a different Hall conductance can be seen as a distinct phase of matter and corresponds to ground states which can not be reached without closing the gap, and respectively going through a plateau at the level of the conductance. One can show that N in Eq.(1) equals n. Furthermore it can be showed that the trivial insulator is equivalent to the vacuum since the vacuum has, according to Diracs's relativistic quantum theory, an energy gap (for the pair production), the electrons forming the conductance band and the positron forming a valence band. One peculiarity of topological insulators is the existence of an insulating bulk and metallic edge states. Let us consider an interface of a material with different Chern numbers for example n=1 and n=0, which can be seen as the interface of a QH material and the vacuum. If we slowly interpolate the gap between the QH state and the vacuum as a function of the distance, somewhere along the interface the energy gap has to vanish, because this is the only possibility for the Chern number to change. This explains the robustness of the quantization of σ_{xy}. The existence of low energy gapless states near the edge is therefore inevitable if the topological invariant changes. Another remarkable fact is that the quantization of σ_{xy} is still accurate in disordered samples. In the integer QHE the Chern number simply is the number of gapless modes at the edge or the value of the Hall conductance in multiples of e^2/h. One says that the edge states are topologically protected by the bulk property. This means that the freedom of the electrons at the edges (moving left or right) is spatially separated on opposite edges. Backscattering at one edge is therefore forbidden due to a lack of electrons moving with the opposite direction of motion. Since the direction of motion of the electrons are fixed (depending on the sign of the magnetic field) they are referred to as chiral.

The QH state belongs to a topological class which breaks time reversal symmetry (TRS), for example due to the presence of magnetic fields. It is therefore natural to ask whether the breaking of time reversal symmetry is a necessary condition for topological nontrivial states. One of the first who theoretically predicted this new phase of matter in two dimensions were Kane and Mele [9] and Bernevig, Andrei and Zhang [10]. In the 2D case it is called Quantum spin hall insulator (QSH) or synonymously 2D topological insulator. The QSH state does not require a magnetic field which leads to the TRS breaking and is expected to have robust quantized properties. It can be seen (approximately) as two copies of the QHE with opposite chiralities at the edge, with one copy for each spin (see figure 1).
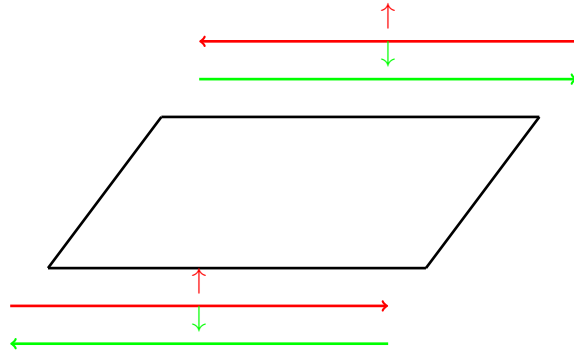

Figure 1: Opposite spins are moving in opposite directions at edges of the QSH material

This gives the same robustness against backscattering as in the QH state, because the backscattering would need to cause a spin flip to backscatter the electron. The resulting edge states are termed as helical, since there is a fixed relation between the electrons momentum and the spin. Since the QSH state is robust to disorder in the presence of TRS and it has an insulating bulk and gapless edge modes it is a new topological state of matter. Because the charge Hall conductance vanishes the Chern number is not good to classify this type of topological insulator. It can be shown that all TR invariant insulators in nature belong to ten different classes, characterized by a either a $\mathbb{Z}$, $\mathbb{Z}_2$ or no topological order parameter [11]. In the 2D case, the $\mathbb{Z}_2$ parameter can take the value 0 or 1. The topologically nontrivial state has a full insulating gap in the bulk , but has gapless edge or surface states consisting of an odd number of Dirac fermions. This can

be seen from figure 2. The T operator is defined as $T = e^{i\pi\sigma_y}\hat{K}$, where σ_y denotes the 2nd Pauli matrix and $\hat{K}$ stands for the complex conjugation. This fulfills our expectation of a time reversal since it flips the spins and inverts the direction of motion $p \to -p$ etc. For spin $1/2$ fermions, T fulfills the property $T^2 = -1$. This leads to an important fact, known as Kramer's theorem, which states that all eigenstates of a T invariant Hamiltonian are at least twofold degenerate. In the absence of spin orbit interaction (SOI) it is simply the degeneracy between up and down spins. In the presence of SOIs, which is part of the model description and needed for the appearance of surface states, it has nontrivial consequences. A T invariant Hamiltonian has to satisfy the following relation $TH(\mathbf{k})T^{-1} = H(-\mathbf{k})$. This holds only at certain points in the Brioullin zone, for example $\Gamma_a = 0$ and $\Gamma_b = \pi/a$. At the T invariant momenta, Kramer's theorem guarantees that the states are twofold degenerate and the T invariance shows that they must have the same energy. Everywhere else the SOI splits up this degeneracy. If the number of surface states is even then one can get rid of them by adiabatically changing the band structure and the position of E_F, whereas this is not possible for an odd number of surface states. If a state is a trivial insulator or not can be seen by looking at the topological class of the bulk band structure (see figure 2). Since TRS guarantees every electron with k to have a partner at -k, we can see the $\mathbb{Z}_2$ invariant is the number of Kramer pairs modulo 2. One can therefore conclude that the 2D topological insulator must have topologically protected edge states. [12] [8]
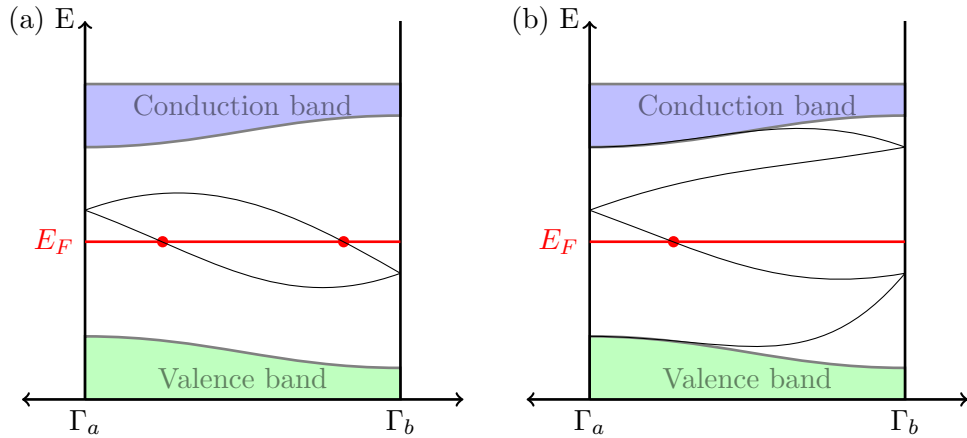
Figure 2: Electronic dispersion between the T invariant momenta $\Gamma_a = 0$ and $\Gamma_b = \pi/a$. The number of surface states crossing E_F is even in (a) and odd in (b). The odd number leads to topologically protected boundary states. Only one half of the BZ is shown, because T symmetry requires the other half to be a mirror image.

The QSH insulator was first experimentally observed in HgTe/CdTe quantum wells by König et al [13]. The QSH in the HgTe/CdTe quantum well is characterized by an insulating bulk and a pair of helical edge states (HES). There is a quantum phase transition when the thickness of the material is under the critical thickness from a topological insulator to a trivial insulator. For the thicker quantum wells they could measure a longitudinal conductance of $2e^2/h$, which corresponds to each edge mode contributing a conductance of e^2/h for each helicity.

More recent approaches to helical systems are based on the formation of interaction induced helical modes in InAs or GaAs quantum wires.

One possible theoretical model which explains for example, the appearance of helical modes in wires is the Kondo chain. It consists of electrons on a one-dimensional lattice, which interact with localized magnetic moments. The indirect exchange interaction, known as Ruderman-Kittel-Kasuya-Yosida interaction, can be found in the second-order perturbation theory, where the magnetic moments of the atoms interact with the spin of the conduction electrons through the hyperfine interaction. This electron can then interact with other nuclear spins, which can lead to a correlation between the nuclear magnetic moments and an ordering of the conduction

electron's spins. Tsvelik and Yevtushenko showed in [3] that there is a phase transition in the wire, due to the spontaneous breaking of $\mathbb{Z}_2$ symmetry between sectors with different helicity of the fermions. The coupling J between the magnetic moment and the electron's spin is considered isotropic in the x-y-plane: $J_x = J_y = J_\perp$. The model shows two different regimes which differ by the predominant direction of the spins orientation under interaction, namely the easy axis (EA), $J_z > J_\perp$, and the easy plane (EP), $J_z < J_\perp$, anisotropy. If the anisotropy has the EA form, the band structure of the wire is gapped. The electrons are localized by the magnetic impurities and the transport of charge, carried by the quasi particle excitations, is therefore blocked. $J_z = J_\perp$ is the point of the quantum phase transition. In the EP phase the quasi particles with a given helicity acquire a gap, whereas the other helical branch remains gapless (see figure 3).
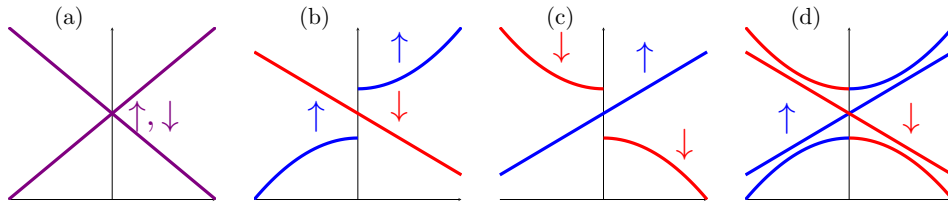

Figure 3: This figure shows the partial gap opening presented in Ref. [3]. The idealized degenerate dispersion relation can be seen in (a). Figure (b) and (c) show that a gap opens for the spin up and spin down particles of a given helicity. The resulting dispersion relation can be seen in (d), where a gap has opened for spin down particles. This corresponds to the breaking of the $\mathbb{Z}_2$ symmetry, since every partner with the momentum k should have a partner at -k with the opposite spin.

If spin conservation is respected in the wire, the helical ordering of the electrons make single-particle backscattering impossible. This leads to a symmetry protection for helical edge states, due to many-body effects comparable to those in the QSH insulator, where the protection arises to the topologically nontrivial bulk. It has been shown in ref. [4], that a new order parameter can be introduced, which distinguishes the EP and the EA phase. This parameter $A_c = \epsilon_{abc}\langle S^a(1)S^b(1+\xi_0)\rangle$ can be written as the average of the vector product of two neighboring spins. For the EA case the S^x and S^y components of the spins are uncorrelated. In the EP case the S^x and S^y components of the spin are correlated and form a helix in the S^x-S^y space

plotted over k_F. The asymmetry between the spontaneously broken helical states can be seen when computing the in-plane susceptibility $\langle S^+(1)S^-(2)\rangle$. In the EA phase it has peaks at $2k_F$ and $-2k_F$, whereas in the EP phase it has a peak only at either $2k_F$ or $-2k_F$, depending on the helix orientation.

One possible experimental realization is a cleaved edge overgrowth GaAs quantum wire, see [2]. Scheller et al showed, that at temperatures above 10 Kelvin the quantum wires showed the quantized conductance $2G_0 = e^2/h$ (one mode of conductance for each spin), which means that the electrons were not gapped. Below 100 mK the conductance showed a drop by the factor of two, which suggests a potential gap opening and spin ordering. This remained constant for further cooling.

Another possible realization can be found in quantum wires with a strong spin-orbit interaction(SOI). This interaction is a relativistic effect, where an electron travelling through an electric field experiences a magnetic field, that interacts with the electron's magnetic moment, in its rest frame. This interaction is the basis for the spin-orbit coupling (SOC), which causes a splitting of the electrons in atoms depending on their spin state. In semiconductor devices, the difference in the conduction-band energies between to different materials give rise to an electric field, which leads to a SOI. The resulting effect is termed Rashba effect. [14]

Quay et al. have shown, that applying magnetic fields along the wire, perpendicular to the magnetic field seen by the electrons from the SOC can open a gap in the dispersion relation, such that, when the Fermi energy lies inside the gap, one gets HES. See figure 4 and ref. [5].
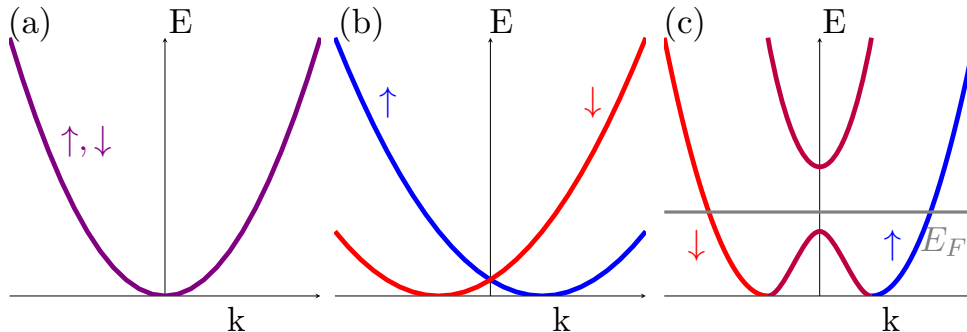
Figure 4: (a) The free electron dispersion relation, which is degenerate for up-and down spins. (b) The dispersion relation under the influence of the SOI. The degeneracy is removed, displacing the spin sub bands with respect to each other. (c) Opening of a SOI gap, when a magnetic field along the length of the wire is applied, which creates a spin mixing of the subband and thus a anticrossing. Tuning E_F to the SOI gap allows one to obtain right moving particles with e.g. spin up and left moving particles with spin down.

Heedt et al measured the conductance of such nanowires and found evidence for the formation of helical states in the lowest 1D subband of InAs wires [1]. The HES appear because of the Rashba SOI. Other than expected it is not necessary to apply an external field perpendicular to the spin-orbit field. Although the effect is enhanced, when a magnetic field is applied to the wire, the field does not seem necessary to open a gap.

2 Motivation and Statement of Problem

Helical states are a hot topic in modern solid state physics. Their unique electronic properties, like the ideal transport of charge or spin, make them a potential candidate for modern electronic semiconductor devices and for quantum computing [8–10, 12]. A possibility to realize HES in 1D wires attracts a growing attention. However, a smoking gun evidence, confirming the helical transport in 1D wires, is still absent [1–5, 15]. It is extremely important to develop reliable tools, which allows one to identify the HES in real experiments. In this thesis, we focus on quantum interference effects, namely the Aharonov-Bohm effect, and look at the peculiarities which arise due to the helical nature of the states. The following questions will be

addressed in this project.

- Will one observe AB-oscillations in a helical ring setup, connected to helical leads?

- Will one observe AB-oscillations in a helical ring setup, connected to non-helical leads?

- Is there a difference between the conductance of the above setups, compared to a normal ring, especially regarding the period of the oscillations?

- Can the AB setup be used to distinguish HES and normal wires?

3 Main part

3.1 The Y-junction of helical wires

In a first attempt to investigate quantum interference effects in helical systems, we want to build an Aharonov-Bohm ring made out of helical quantum wires. A basic element of the circuit is the beam splitter which divides and merges the electrons into two paths (see Figure 5). This Y-junction consists of 3 wires with different helicities of the wires. We can think of two different setups. One where the outgoing arms have equal chirality, which we will denote as S_a setup, and one where they have different chirality, which will be denoted as S_b. Figure 5 shows the labeling of our states.

We use the S-matrix formalism to find a possible solution for the Y-junction. Our system provides three transport channels and therefore, we need a 3x3 S-Matrix [16]. The S-Matrix has the general form:

$$S = \begin{pmatrix} r_{11} & t_{12} & t_{13} \\ t_{21} & r_{22} & t_{23} \\ t_{31} & t_{32} & r_{33} \end{pmatrix}, \tag{3}$$

where r_{ii} is the amplitude of the following process: the electron approaching the junction in the transport channel i is reflected back to the same channel i. Consequently, $|r_{ii}|^2$ is the probability of this process. t_{ij} is the amplitude of the following process: the electron approaching the junction in the transport channel i is transmitted in the channel j, with $|t_{ij}|^2$ being the probability of this process. The scattering matrix relates the in going and outgoing states in the following way: $\psi_{out} = S\psi_{in}$. To guarantee the conservation of the particle number, we require the reflection and transmission probabilities in
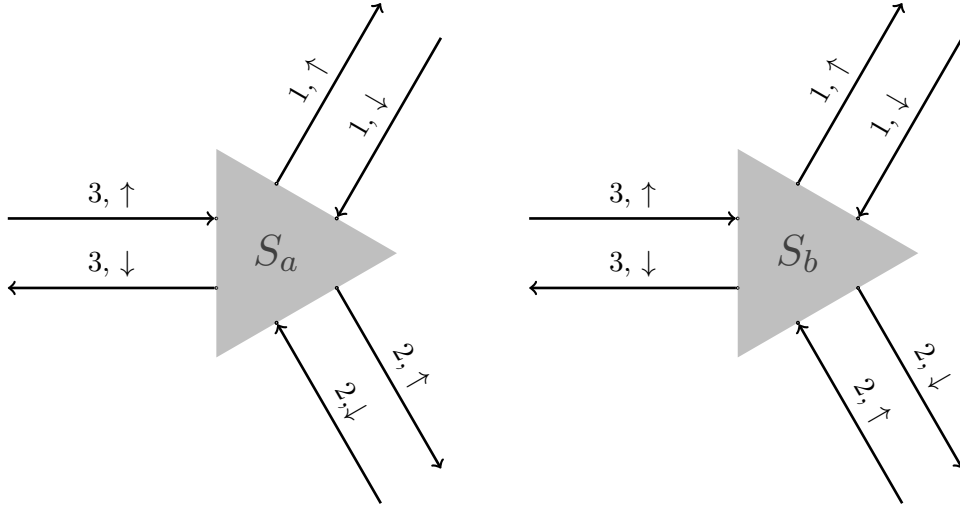
Figure 5: Channel number and helicity of two different beam splitters.

each channel to add up to one, which is equivalent to the statement that our S-Matrix is unitarity:

$$SS^\dagger = S^\dagger S = \mathbb{1}. \tag{4}$$

Equipped with this knowledge, one can try to guess the correct S-matrix for the helical Y-junction, which fulfills the requirements above. In helical wires, we expect no backscattering, since there is no transport channel which carries electrons with the opposite velocity, but with the same spin. Furthermore we exclude electron-electron interaction which could cause a spin flipping during the scattering process. This helps us to restrict the S-Matrix, because we can assume that the diagonal entries of the S-matrix have to be zero.

S_a setup

Since channel two has no outgoing mode with spin down, the probability of transmission in this channel from channel one is zero. Following this pattern, checking if $t_{ij} \neq 0$, simply from the matching of the spins of the in states and out states, gives us the S-Matrix:

14

$$S = \begin{pmatrix} 0 & 0 & t_{13} \\ 0 & 0 & t_{23} \\ t_{31} & t_{32} & 0 \end{pmatrix}. \tag{5}$$

An attempt to check the unitarity condition, yields:

$$SS^\dagger = \begin{pmatrix} 0 & 0 & t_{13} \\ 0 & 0 & t_{23} \\ t_{31} & t_{32} & 0 \end{pmatrix} \cdot \begin{pmatrix} 0 & 0 & t_{31}^* \\ 0 & 0 & t_{32}^* \\ t_{13}^* & t_{23}^* & 0 \end{pmatrix} = \begin{pmatrix} t_{13}t_{13}^* & t_{13}t_{23}^* & 0 \\ t_{23}t_{13}^* & t_{23}t_{23}^* & 0 \\ 0 & 0 & t_{31}t_{31}^* + t_{32}t_{32}^* \end{pmatrix},$$

which obviously can never be equal to $\mathbb{1}$. Therefore, a unitary S-Matrix cannot be constructed.

S_b setup

Since channel two has no outgoing mode with spin up the probability of transmission in this channel from channel three is zero. Analog to the setup above, we get the S-Matrix through checking if scattering from one channel into another is possible or not. This gives:

$$S = \begin{pmatrix} 0 & t_{12} & t_{13} \\ t_{21} & 0 & 0 \\ t_{31} & 0 & 0 \end{pmatrix}. \tag{6}$$

An attempt to check the unitarity condition, yields:

$$SS^\dagger = \begin{pmatrix} 0 & t_{12} & t_{13} \\ t_{21} & 0 & 0 \\ t_{31} & 0 & 0 \end{pmatrix} \cdot \begin{pmatrix} 0 & t_{21}^* & t_{31}^* \\ t_{12}^* & 0 & 0 \\ t_{13}^* & 0 & 0 \end{pmatrix} = \begin{pmatrix} t_{12}t_{12}^* + t_{13}t_{13}^* & 0 & 0 \\ 0 & t_{21}t_{21}^* & t_{21}t_{31}^* \\ 0 & t_{31}t_{21}^* & t_{31}t_{31}^* \end{pmatrix},$$

which obviously can never be equal to $\mathbb{1}$. Therefore, a unitary S-Matrix cannot be constructed.

Almost helical S-Matrix

In a second attempt (Appendix B), we have analyzed a possible parameterization for a S-Matrix which requires all reflection coefficients to be zero. The result is a matrix which shows that single transport channels have to be connected with perfect transmission. In the case of the full helical Y-junction, one possible experimental result could be that two wires are connected with perfect transmission, whereas the third wire is disconnected from the whole setup.

3.2 Conductance of the normal-helical-normal setup

In this section, we will further investigate the AB-effect on HES systems. To understand the AB-effect, we consider a one-dimensional motion e.g. in a certain transport channel. If an electron travels through a region with a smooth electromagnetic potential $V(x,t)$, such that no scattering occurs, it acquires a phase. The Hamiltonian of this system reads $H = H_0 + V(x,t)$, where H_0 is the Hamiltonian without an extra potential. If Ψ_0 is a solution for H_0, then the solution for H will be

$$\Psi = \Psi_0 e^{-i\Theta/\hbar}, \quad \Theta = \int V(x,t)dt, \tag{7}$$

which can be seen from inserting this in the Schrödinger equation. If we consider a setup, where the electrons are split up into two different paths, their wave function can be written as

$$\Psi = \Psi_{0,1} e^{-i\Theta_1/\hbar} + \Psi_{0,2} e^{-i\Theta_2/\hbar}, \tag{8}$$

$$\Theta_1 = \int V_1(x,t)dt, \quad \Theta_2 = \int V_2(x,t)dt. \tag{9}$$

It is apparent, that the interference of the two parts at some point will depend only on the phase difference $\Theta_1 - \Theta_2$. Thus, there is a physical effect of the potentials even though no force ever acts on the electron. As noticed by Aharonov and Bohm 1959, there are two different contributions depending on the form of the potential. The phase shift depending on the electric potential yields:

$$\Delta\Theta_{el} = e \int \Phi_{el} dt \tag{10}$$

This phase shift due to potential is called dynamical phase. It has an important property: if an electron takes a time-reversed path, lets say from x_2 to x_1, the phase shift accumulated is the same as going from x_1 to x_2. In contrast to this, the phase shift due to magnetic fields are more complicated. The magnetic phase accumulated along the trajectory depends on the vector potential $\mathbf{A}(x)$ and is opposite for the time reversed path.

$$\Delta\Theta_{mag} = \frac{e}{c} \int \mathbf{A} d\mathbf{x}. \tag{11}$$

Shifting the vector potential by an arbitrary gradient $\mathbf{A} \to \mathbf{A} + \nabla\chi(x)$ field will lead to precisely the same physical situation. The phase shift will depend

explicitly on $\chi(x)$, which makes it unobservable. The phase difference can also be evaluated as the integral around a closed circuit in space time, where the potentials are evaluated at the place of the center of the wave packet. This gauge-invariant observable quantity is the magnetic phase accumulated along a closed path, where the electron returns to the same point. It is proportional to the magnetic flux Φ enclosed by this trajectory,

$$\Delta\Theta_{mag} = \frac{e}{c} \oint \mathbf{A} d\mathbf{x} = \frac{e}{c} \int \mathbf{B} d\mathbf{A} = \frac{2\pi\phi}{\phi_0}, \qquad (12)$$

where $\phi_0 = hc/e$ is the magnetic flux quantum. In general, any periodic dependence on ϕ/ϕ_0 is called Aharonov-Bohm (AB) effect [16, 17].

We consider a setup of an Aharonov-Bohm ring which provides helical edge states connected to metallic non-helical leads. The calculation basically follows Maciejko et al [18], who looked at a ring made of a QSH insulator material connected to spin polarized metal leads. Let us emphazise the difference between Maciejko's paper and this project. The metal lead in our setup is modelled as the combination of two helical edge states with different chirality. This means that, in contrast to the paper [18], we only consider full loop contributions (figure 6), since only electrons with the same spin contribute to the conductance in the same transport channel.
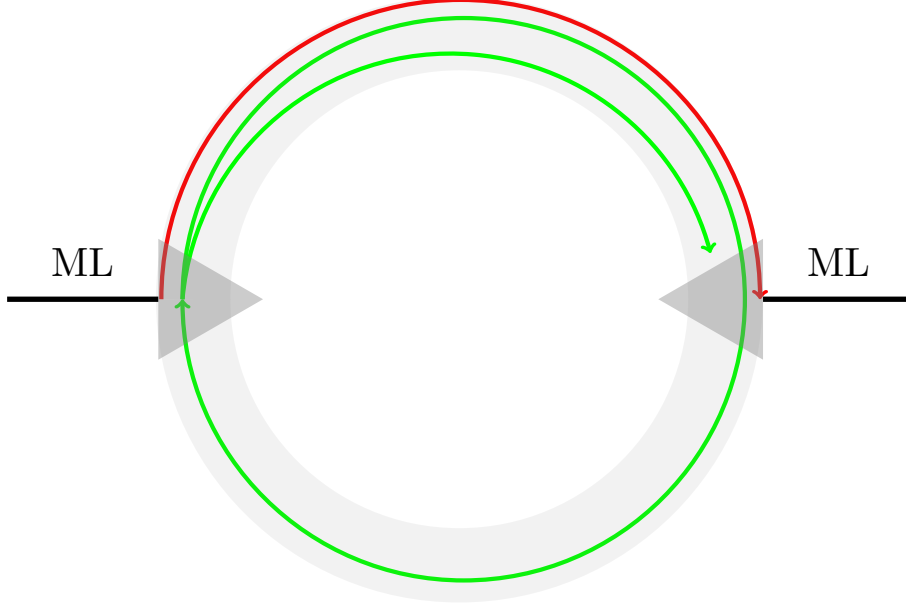
17

Figure 6: Phenomenological analysis of the interference paths: Since spin up can only go clockwise in our setup (depends on the convention we took), there is only one possible type of interference (Same for spin down, but going counterclockwise). The red path shows a half-loop, the phase shift gathered here is equal to $\lambda + \Theta_1$, where λ stands for the dynamical phase. The green path shows one and a half loop, the phase shift is equal to $2(\lambda + \Theta_1) + \lambda + \Theta_2$. Even the interference of these two trajectories yields the AB-effect. The transmission probability contains an interference term of the form $P_{red,green} = 2Re[t_{red}t_{green}^*] \propto \cos(2\lambda + \Theta_1 + \Theta_2) = \cos(2\lambda + \Theta_{AB})$. Contributions of this type depend on the dynamically phase and underlie universal conductance fluctuations, because for identical nanostructures, these phase shifts are random. So, this contribution is individual for each nanostructure and will disappear, if we average over a large ensemble of nominally identical ones [16].

This is a difference to Ref. [18] since it addresses spins mixing at the junction, where the HES are connected to spin full polarized wires.

Our scattering problem at the junction is therefore equivalent to a helical X-junction or corner junction. We have four in going helical states and four outgoing helical states, where two helical states form our non-helical metallic lead, since, in combination, they transport spin up and down in every

direction. This can be seen in Figure 7. We want to obtain an expression for the 4x4 S-matrix S which relates the in going amplitudes to the outgoing amplitudes in the form:

$$\begin{pmatrix} m_{l,\uparrow} \\ m_{l,\downarrow} \\ m_{r,\uparrow} \\ m_{r,\downarrow} \end{pmatrix}_{out} = S \begin{pmatrix} m_{l,\uparrow} \\ m_{l,\downarrow} \\ m_{r,\uparrow} \\ m_{r,\downarrow} \end{pmatrix}_{in} \quad with \quad S = \begin{pmatrix} r & t' \\ t & r' \end{pmatrix}, \tag{13}$$

where m_l and m_r are the current amplitudes far from the junction. The S-matrix has therefore the dimensions 4×4. The submatrices r, r', t, t' are 2×2 matrices and describe the reflection and transmission of a given state. Our Aharonov-Bohm ring consists of a left beam splitter, which divides the electron's path in an upper and a lower arm, and a right beam splitter, which merges the beams again. Between the upper and lower arm we place a magnetic flux confined to a long solenoid. We define the scattering matrices S_L and S_R for the left and right junction of the ring. They relate the amplitudes at the junction in the following way (see figure 7):

$$\begin{pmatrix} m_{\uparrow} \\ m_{\downarrow} \\ h_{\uparrow} \\ h_{\downarrow} \end{pmatrix}_{out,left} = S_L \begin{pmatrix} m_{\uparrow} \\ m_{\downarrow} \\ h_{\uparrow} \\ h_{\downarrow} \end{pmatrix}_{in,left} \quad , \quad \begin{pmatrix} h_{\uparrow} \\ h_{\downarrow} \\ m_{\uparrow} \\ m_{\downarrow} \end{pmatrix}_{out,right} = S_R \begin{pmatrix} h_{\uparrow} \\ h_{\downarrow} \\ m_{\uparrow} \\ m_{\downarrow} \end{pmatrix}_{in,right}$$
$$\tag{14}$$

Here m and h refer to the two-component spinors of the metallic lead's and the helical edge state's current amplitudes. This is equal to unfolding the setup in the following way. This can be seen in figure 8.
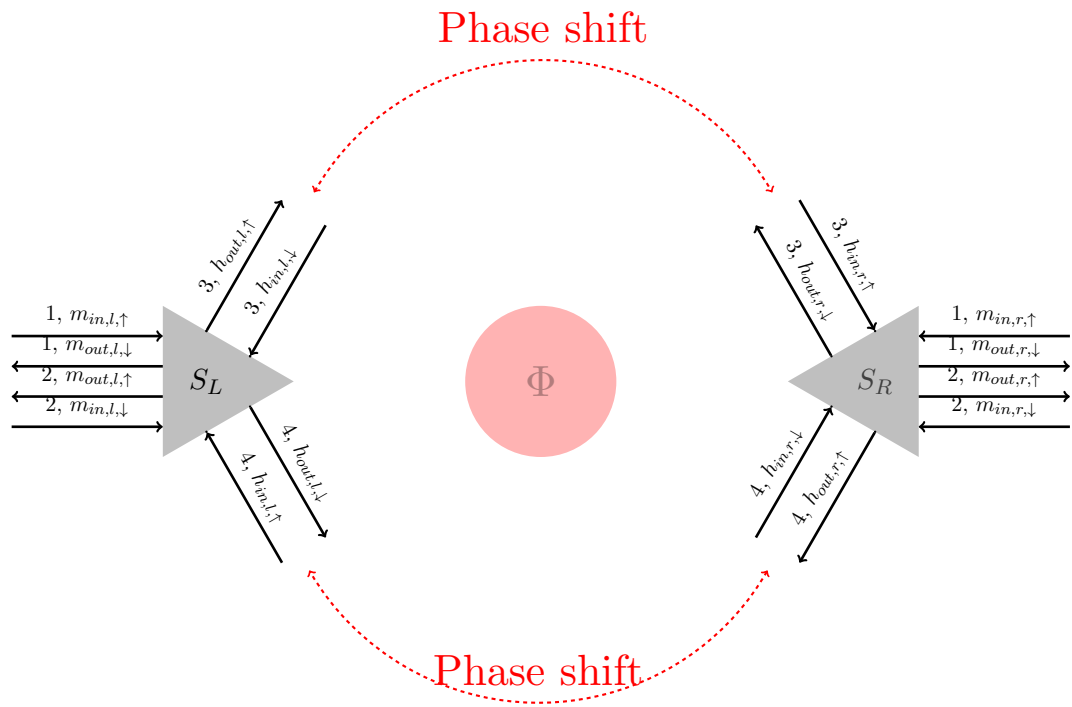
Figure 7: In- and out states of the Aharonov-Bohm ring

$$\Psi_{in,left} = \begin{pmatrix} m_\uparrow \\ m_\downarrow \\ h_\uparrow \\ h_\downarrow \end{pmatrix} \quad \Psi_{out,left} = \begin{pmatrix} m_\uparrow \\ m_\downarrow \\ h_\uparrow \\ h_\downarrow \end{pmatrix} \quad \Psi_{in,right} = \begin{pmatrix} h_\uparrow \\ h_\downarrow \\ m_\uparrow \\ m_\downarrow \end{pmatrix} \quad \Psi_{out,right} = \begin{pmatrix} h_\uparrow \\ h_\downarrow \\ m_\uparrow \\ m_\downarrow \end{pmatrix}$$
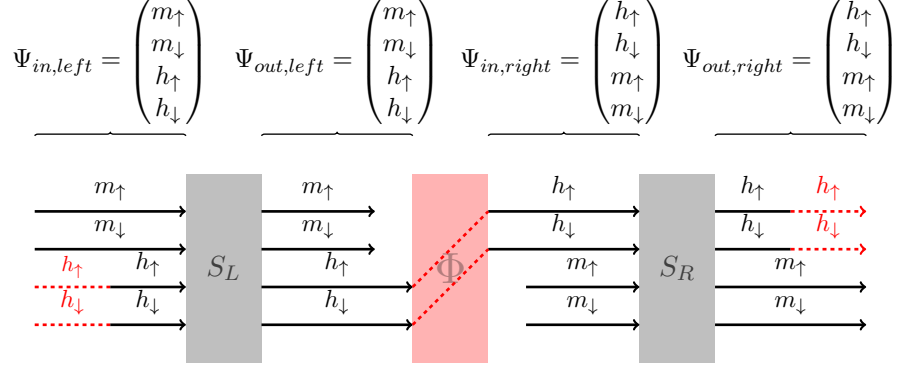
Figure 8: Unfolding of the Aharonov-Bohm ring scattering problem. $m_{\uparrow,\downarrow}$ stands for the HES in the metallic leads. $h_{\uparrow,\downarrow}$ denote the HES in the helical wire. The red dotted lines indicate the phase shift between the out states of the left scattering matrix and the in states of the right scattering matrix and the other way round.

The amplitudes are related through the Aharonov-Bohm phase $\varphi = 2\pi\phi/\phi_0$, where ϕ is the magnetic flux and $\phi_0 = hc/e$ is the flux quantum, which is opposite for each spin polarization due to the fact, that spin up electrons only pass the ring clockwise, whereas spin down electrons go anticlockwise. The arms are symmetric in length. The dynamical phase $\lambda = 2k_F l$ is the same for both electron spins, l being the distance traveled by the edge electrons from the left to right junction and k_F being the edge-state Fermi wave vector. The helical in-states of the right and left beam splitter are the helical out-states from the left and right beam splitter related through the phase shift in the following way:

$$\begin{Bmatrix} h_{r,\uparrow,\downarrow} \\ h_{l,\uparrow,\downarrow} \end{Bmatrix}_{in} = e^{i\frac{\lambda}{2}} e^{\mp i\frac{\varphi}{2}} \begin{Bmatrix} h_{l,\uparrow,\downarrow} \\ h_{r,\uparrow,\downarrow} \end{Bmatrix}_{out}, \tag{15}$$

where the upper sign corresponds to spin up. Using Eq.(14) and Eq.(15) gives us

$$\begin{pmatrix} e^{-i\frac{\lambda}{2}}\Phi^\dagger h_{l,in} \\ m_{r,out} \end{pmatrix} = S_R \begin{pmatrix} e^{i\frac{\lambda}{2}}\Phi h_{l,out} \\ m_{r,in} \end{pmatrix}, \tag{16}$$

where we define $\Phi \equiv e^{-i\varphi\frac{\sigma_z}{2}}$, with σ_z being the Pauli matrix. Using the first term in Eq.(14) together with Eq.(16) allows us to eliminate the amplitudes

$h_{l,in}, h_{l,out}$ and obtain the relations between $m_{l,in}, m_{l,out}, m_{r,in}, m_{r,out}$. This yields the S-Matrix.

From the relations

$$\begin{pmatrix} m \\ h \end{pmatrix}_{out,left} = S_L \begin{pmatrix} m \\ h \end{pmatrix}_{in,left}, \quad \begin{pmatrix} e^{-i\frac{\lambda}{2}}\Phi^\dagger h_{l,in} \\ m_{r,out} \end{pmatrix} = S_R \begin{pmatrix} e^{i\frac{\lambda}{2}}\Phi h_{l,out} \\ m_{r,in} \end{pmatrix}, \quad (17)$$

we obtain (see Appendix C)

$$t = t_R[\mathbb{1} - e^{i\lambda}\Phi r'_L \Phi r_R]^{-1}\Phi e^{i\frac{\lambda}{2}} t_L. \tag{18}$$

The conductance of the ring can be determined by using the Landauer formula. Eq.(51) expresses G in terms of the scattering matrices at the junctions. As before, we use rather heuristic methods to guess the right S-matrix (for the construction see the figure 8). The convention we took for the in- and out-states gives a S-matrix of the form

$$S = \begin{pmatrix} r_1 & 0 & t_1 & 0 \\ 0 & r_2 & 0 & t_2 \\ t_3 & 0 & r_3 & 0 \\ 0 & t_4 & 0 & r_4 \end{pmatrix}. \tag{19}$$

A further restriction for this matrix appears if the system has TRS. The time reversal operator, is $T = e^{i\pi\sigma_y}\hat{K}$, where σ_y denotes the second Pauli matrix and $\hat{K}$ stands for the complex conjugation, acting on the in-states and out-states gives the following relations $T\Psi_{in(out)} = Q\Psi_{out(in)}$, with Q $= \mathbb{1} \otimes \sigma_y$. This results in the following relation $S = -QS^T Q$ [19, 20]. This leads to a S-matrix, up to an overall phase, in the form of

$$S = \begin{pmatrix} r_1 & 0 & t_1 & 0 \\ 0 & r_1 & 0 & t_2 \\ t_2 & 0 & r_3 & 0 \\ 0 & t_1 & 0 & r_3 \end{pmatrix}. \tag{20}$$

The unitarity condition reads

$$SS^\dagger = \begin{pmatrix} r_1 r_1^* + t_1 t_1^* & 0 & r_1 t_2^* t_1 r_2^* & 0 \\ 0 & r_1 r_1^* + t_2 t_2^* & 0 & t_2 r_2^* + r_1 t_1^* \\ t_2 r_1^* + r_2 t_1^* & 0 & r_3 r_3^* + t_2 t_2^* & 0 \\ 0 & r_2 t_2^* + t_1 r_1^* & 0 & r_3 r_3^* + t_1 t_1^* \end{pmatrix} = \mathbb{1}. \tag{21}$$

We choose $r = r_1 = r_3^*$ and $t = t_2 = -t_1^*$ to fulfill Eq.(21) and obtain

22

$$S = \begin{pmatrix} r & 0 & -t^* & 0 \\ 0 & r & 0 & t \\ t & 0 & r^* & 0 \\ 0 & -t^* & 0 & r^* \end{pmatrix}. \qquad (22)$$

The conductance G takes the form (see Appendix D)

$$G = \frac{2e^2}{h} t_R t_R^\dagger t_L t_L^\dagger \left(\frac{1}{1 - e^{i(\lambda-\varphi)} r_R r_L^* - e^{-i(\lambda-\varphi)} r_R^* r_L + |r_R|^2 |r_L|^2} + \right. \qquad (23)$$

$$\left. + \frac{1}{1 - e^{i(\lambda+\varphi)} r_R r_L^* - e^{-i(\lambda+\varphi)} r_R^* r_L + |r_R|^2 |r_L|^2} \right).$$

We now consider a symmetric setup with an inversion symmetry. The conductance should not change if we send a current from the right or left through the AB-ring. This means that $r_R = r_L = a$ and $t_R = t_L = b$. This leads to further simplifications in the conductance.

$$G = \frac{2e^2 |b|^4}{h} \frac{1}{1 - 2|a|^2 cos(\lambda - \varphi) + |a|^4} + \frac{1}{1 - 2|a|^2 cos(\lambda + \varphi)|a|^4}. \qquad (24)$$
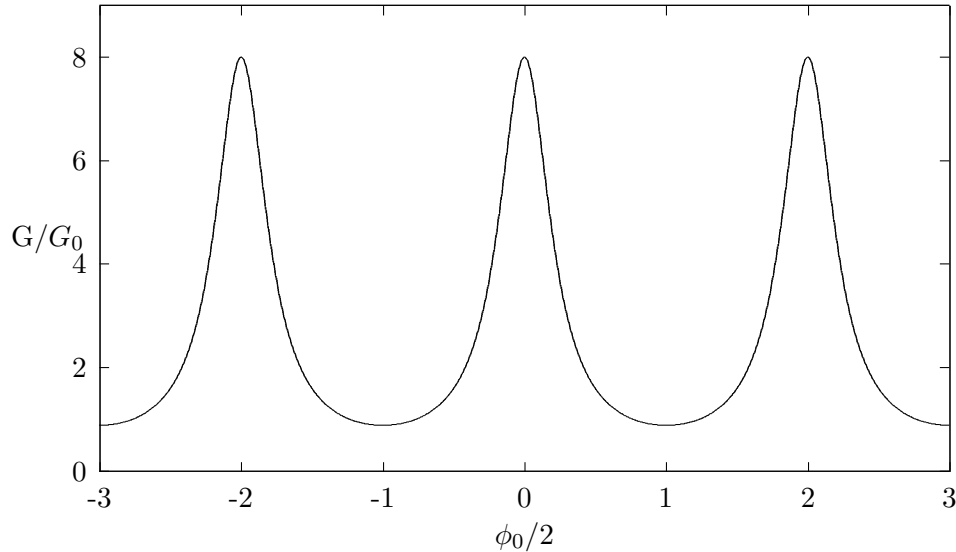
Figure 9: Conductance for the specific set of parameters $|a|^2 = 1/2$, $|b|^2 = 1/2$, $\lambda = 0$

An example of the AB-oscillations is shown in figure 9. We can see that the conductance of the Aharonov-Bohm ring is $2\pi-$periodic in φ, and therefore periodic in the magnetic flux with a period of ϕ_0. This is in compliance with Ref. [18], despite of different interfering trajectories, in the case of vanishing magnetization of the wire.

4   Conclusion and main results

In this work, we have analyzed the quantum interference effect, namely the AB effect, in different setups which can be used to distinguish normal wires from the recently found helical wires. Our theoretical results can be used as an additional tool confirming the existence of interaction induced helical states. The main result of this work are:

- In Section 3.1, we have shown that there is no possible solution for a full helical Y-beamsplitter, one basic component of the AB-ring, under the assumption, that the S-matrix conserves the particle number and the spin. Therefore, if one tries to build an Aharanov-Bohm ring made

24

entirely out of helical wires, it should not be possible to see any AB-oscillations. The absence of the AB-oscillations in the purely helical setup may confirm the helical nature of the electrons.

- In section 3.2, we have considered an Aharonov-Bohm ring connected to normal non-helical metallic leads. We have shown that, if the arms of the AB-ring have opposite chirality, then one can see AB-oscillations with a period of $\varphi = 2\pi\phi/\phi_0 = 2\pi$. This means that the oscillations are periodic in the magnetic flux send through the ring with a period of ϕ_0, integer multiples of the flux quantum. The HES's behavior is similar to the AB-oscillations in normal wires or to the oscillations in the QSH material [18].

- If the arms of the ring have the same chirality, then there are no oscillations. The S-Matrix of the System would take the same form as the S-Matrices in section 3.1 plus an additional 4th wire, which is not connected to anything

The absence of oscillations in the normal-helical-normal setup with equal chirality can also be used to distinguish helical wires from normal wires. Recent studies have shown that the HES can originate from spontaneous symmetry breaking [4]. If one manufactures Aharonov-Bohm rings, the chirality of the arms would be uncontrollable random. If a sufficiently large number of rings is produced, both setups, with equal and opposite chirality of the arms, should appear with the same probability. The setup with equal chirality of the arms should show no AB-oscillations. The setup with opposite chirality of the arms should show AB-oscillations with a period of ϕ_0. Therefore, the probability to see oscillations in a large number of nominally identical experiments is a proof for the helical nature of the 1D wires.

5 Acknowledgment

References

[1] S. Heedt *et al.*, " Signatures of interaction-induced helical gaps in nanowire quantum point contacts," *Nature Physics*, vol. advance online publication, Mar. 2017.

[2] C. P. Scheller *et al.*, " Evidence for Helical Nuclear Spin Order in GaAs Quantum Wires," *Phys. Rev. Lett.*, vol. 112, no. 066801, 2014.

[3] A. M. Tsvelik and O. M. Yevtushenko, "Quantum Phase Transition and Protected Ideal Transport in a Kondo Chain," *Phys. Rev. Lett.*, vol. 115, Nov. 2015.

[4] D. H. Schimmel, A. M. Tsvelik, and O. M. Yevtushenko, "Low energy properties of the Kondo chain in the RKKY regime," *New J. Phys.*, vol. 18, May 2016.

[5] C. H. L. Quay *et al.*, " Observation of a one-dimensional spin–orbit gap in a quantum wire," *Nature Physics*, vol. 6, Mar. 2010.

[6] L. Landau, "On the theory of phase transitions," *Zh. Eksp. Teor. Fiz.*, vol. 7, pp. pp. 19–32, 1937.

[7] K. von Klitzing, "The quantized Hall effect," *Rev. Mod. Phys.*, vol. 58, July 1986.

[8] X.-L. Qi and S.-C. Zhang, "Topological insulators and superconductors," *Rev. Mod. Phys.*, vol. 83, Oct. 2011.

[9] C. Kane and E. J. Mele, "Z_2 Topological Order and the Quantum Spin Hall Effect," *Phys. Rev. Lett.*, vol. 95, Sept. 2005.

[10] B. A. Bernevig and S.-C. Zhang, "Quantum Spin Hall Effect," *Phys. Rev. Lett.*, vol. 96, Mar. 2006.

[11] A. P. Schnyder, S. Ryu, A. Furusaki, and A. W. W. Ludwig, "Classification of topological insulators and superconductors in three spatial dimensions," *Phys. Rev. B*, vol. 78, Nov. 2008.

[12] C. Kane and M. Z. Hasan, "Colloquium: Topological insulators," *Rev. Mod. Phys.*, vol. 82, Nov. 2010.

[13] M. König *et al.*, "Quantum Spin Hall Insulator State in HgTe Quantum Wells," *Science*, vol. 318, pp. pp. 766–770, Nov. 2007.

[14] K. Richter, "Viewpoint: The ABC of Aharonov Effects," *Physics*, vol. 58, Feb. 2012.

[15] D. Loss, "Nuclear magnetism and electron order in interacting one-dimensional conductors," *Phys. Rev. B*, vol. 80, Oct. 2009.

[16] Y. V. Nazarov and Y. M. Blanter, *Quantum Transport: Introduction to Nanoscience* . Cambridge University Press, May 2009.

[17] Y. Aharonov and D. Bohm, "Significance of Electromagnetic Potentials in the Quantum Theory," *Phys. Rev.*, vol. 115, Aug. 1959.

[18] J. Maciejko, Eun-Ah Kim, and X.-L. Qi, "Spin Aharonov-Bohm effect and topological spin transistor," *Phys. Rev. B*, vol. 82, Nov. 2010.

[19] D. N. Aristov and R. A. Niyazov, "Tunneling into and between helical edge states : Fermionic approach," *Phys. Rev. B*, vol. 94, July 2016.

[20] J. C. Y. Teo and C. Kane, "Critical behavior of a point contact in a quantum spin Hall insulator," *Phys. Rev. B*, vol. 79, June 2009.

[21] D. N. Aristov, "Constraints on conductances for Y-junctions of quantum wires," *Phys. Rev. B*, vol. 83, Mar. 2011.

[22] D. N. Aristov and P. Wölfle, "Transport properties of a Y junction connecting to Luttinger liquid wires," *Phys. Rev. B*, vol. 84, Oct. 2011.

[23] D. N. Aristov and P. Wölfle, "Chiral Y junction of Luttinger liquid wires at strong coupling: Fermionic representation," *Phys. Rev. B*, vol. 88, Aug. 2013.

6   Appendices

A   The Landauer formula

One can describe the transport properties of a multi-terminal nanostructure by using the scattering approach. Our finite-size scattering region is connected to 3 reservoirs (kept at fixed voltages V_1, V_2, V_3). The wave functions in the waveguides are described as plane waves. For each waveguide α we now introduce a set of local coordinates $x_\alpha > 0, y_\alpha, z_\alpha$, where x_α is directed along the waveguide from the scattering region to the reservoir. If we consider a current flowing through the cross section of the waveguide α in the direction from the scattering region to the reservoir, the electrons with $k_x < 0$ originated from reservoir α, are described by the distribution function $f_\alpha(E)$. The electrons with $k_x > 0$ come from various reservoirs(see figure 10).
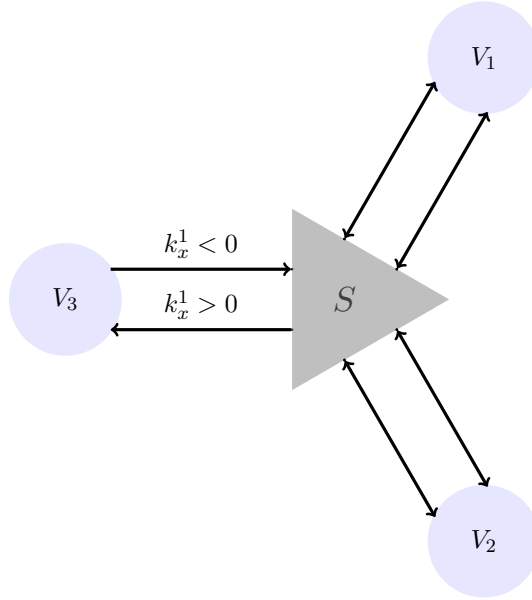

Figure 10: Labeling of k_x.

The fraction of particles that are incident from the reservoir β in the transport channel m and that end up in the waveguide α in the transport channel n, is given by $|S_{\alpha n, \beta m}|^2$, their distribution function being $f_\beta(E)$. The filling factor is given by

$$\sum_{\beta m} |S_{\alpha n, \beta m}|^2 f_\beta(E) \tag{25}$$

We can write the current in terminal α as follows

$$I_\alpha = 2_s e \sum_n \left(\int_{-\infty}^0 \frac{dk_x}{2\pi} v_x(k_x) f_\alpha(E) + \int_0^\infty \frac{dk_x}{2\pi} v_x(k_x) \sum_{\beta m} |S_{\alpha n, \beta m}|^2 f_\beta(E) \right)$$

$$= 2_s e \sum_n \int_0^\infty \frac{dk_x}{2\pi} v_x(k_x) \sum_{\beta m} \left(|S_{\alpha n, \beta m}|^2 - \delta_{\alpha\beta}\delta_{mn} \right) f_\beta(E). \tag{26}$$

Changing variables from k_x to E gives:

$$I_\alpha = -\frac{G_Q}{e} \int_0^\infty dE \sum_{\beta mn} \left(\delta_{\alpha\beta}\delta_{mn} - |S_{\alpha n, \beta m}|^2 \right) f_\beta(E)$$

$$= -\frac{G_Q}{e} \int_0^\infty dE \sum_\beta Tr \left[\delta_{\alpha\beta} - S_{\alpha\beta}^\dagger S_{\alpha\beta} \right] f_\beta(E), \tag{27}$$

where the trace is taken over the transport channels n and m. The matrix $S_{\alpha\beta}$ is a block of the matrix S, which describes the transmission of electrons from terminal β to terminal α (for $\alpha \neq \beta$) or their reflection back to α (for $\alpha = \beta$) [16].

The unitarity condition guarantees the current conservation. The current of all terminals add up to zero, which is consistent with Kirchoff's first law, $\sum_\alpha I_\alpha = 0$. We keep all chemical potentials equal to the Fermi energy, except for one terminal γ, $\mu_\gamma = E_F + eV_\gamma$. This voltage induces a current in all other terminals. The only surviving term in the sum in Eq.(27) is then for $\beta = \gamma$. We obtain $I_\alpha = G_{\alpha\gamma} V_\gamma$ with

$$G_{\alpha\gamma} = -G_Q Tr \left[\delta_{\alpha\gamma} - S_{\alpha\gamma}^\dagger S_{\alpha\gamma} \right], \tag{28}$$

which is referred to as the multi-terminal Landauer equation.

B General parameterization of a S-Matrix

A general parameterization for the S-Matrix has been done to understand at which point the unitarity of the S-Matrix contradicts the assumption of a full helical beam splitter. An arbitrary S-matrix can be represented, up to an overall phase, as follows [21]:

$$S = U e^{i\lambda_5\theta} U' e^{i\lambda_8\alpha_4\frac{\sqrt{3}}{2}},$$

$$U = e^{i\lambda_3\frac{\alpha_2}{2}} e^{i\lambda_2\frac{\chi}{2}} e^{i\lambda_3\frac{\Psi}{2}}, \qquad (29)$$

$$U' = e^{i\lambda_3\frac{\phi'}{2}} e^{i\lambda_2\frac{\chi'}{2}} e^{i\lambda_3\frac{\alpha_3}{2}}.$$

Here the λ matrices are called Gell-Mann matrices

$$\lambda_1 = \begin{pmatrix} 0 & 1 & 0 \\ 1 & 0 & 0 \\ 0 & 0 & 0 \end{pmatrix}, \quad \lambda_2 = \begin{pmatrix} 0 & -i & 0 \\ i & 0 & 0 \\ 0 & 0 & 0 \end{pmatrix}, \quad \lambda_3 = \begin{pmatrix} 1 & 0 & 0 \\ 0 & -1 & 0 \\ 0 & 0 & 0 \end{pmatrix}$$

$$\lambda_4 = \begin{pmatrix} 0 & 0 & 1 \\ 0 & 0 & 0 \\ 1 & 0 & 0 \end{pmatrix}, \quad \lambda_5 = \begin{pmatrix} 0 & 0 & -i \\ 0 & 0 & 0 \\ i & 0 & 0 \end{pmatrix}, \quad \lambda_8 = \frac{1}{\sqrt{3}} \begin{pmatrix} 1 & 0 & 0 \\ 0 & 1 & 0 \\ 0 & 0 & -2 \end{pmatrix} \qquad (30)$$

$$\lambda_6 = \begin{pmatrix} 0 & 0 & 0 \\ 0 & 0 & 1 \\ 0 & 1 & 0 \end{pmatrix}, \quad \lambda_7 = \begin{pmatrix} 0 & 0 & 0 \\ 0 & 0 & -i \\ 0 & i & 0 \end{pmatrix},$$

and $\theta, \alpha_2, \alpha_3, \alpha_4, \chi, \chi', \Psi, \phi'$ are Euler angles. If we consider the limit of linear conductances, it is possible to rewrite the Landauer equation in terms of density matrices. The current in the jth wire is given by $I_j(x) = ev_f [\langle \rho_{j,in}(x) \rangle - \langle \rho_{j,out}(-x) \rangle]$. The linear response theory yields $I_j(x) = \int_{-\infty}^{0} dy \, [\langle \rho_{j,in}(x)\rho_k(y) \rangle - \langle \rho_{j,out}(-x)\rho_k(y) \rangle] V_k$. In the static limit the response function can be evaluated as $G_{jk} = \delta_{jk} - Tr[\rho_{j,out}\rho_{j,in}] = \delta_{jk} - |S_{jk}|^2$ [22]. For a multiplet of incoming fermions $\Psi = (\psi_1, \psi_2, \psi_3)$, the incoming density $\rho_j = \Psi^\dagger \hat{\rho} \Psi$ is given by the simple diagonal matrix

$$\hat{\rho}_1 = \begin{pmatrix} 1 & 0 & 0 \\ 0 & 0 & 0 \\ 0 & 0 & 0 \end{pmatrix}, \quad \hat{\rho}_2 = \begin{pmatrix} 0 & 0 & 0 \\ 0 & 1 & 0 \\ 0 & 0 & 0 \end{pmatrix}, \quad \hat{\rho}_3 = \begin{pmatrix} 0 & 0 & 0 \\ 0 & 0 & 0 \\ 0 & 0 & 1 \end{pmatrix}. \qquad (31)$$

We can rewrite the density matrices in terms of the Gell-Mann matrices. Which gives

$$\hat{\rho}_1 = \frac{1}{2}(\sqrt{\frac{2}{3}}\lambda_0 + \frac{1}{\sqrt{3}}\lambda_8 + \lambda_3),$$

$$\hat{\rho}_2 = \frac{1}{2}(\sqrt{\frac{2}{3}}\lambda_0 + \frac{1}{\sqrt{3}}\lambda_8 - \lambda_3), \qquad (32)$$

$$\hat{\rho}_3 = \frac{1}{\sqrt{6}}\lambda_0 - \frac{1}{\sqrt{3}}\lambda_8.$$

Here $\lambda_0 = \sqrt{\frac{2}{3}}\mathbb{1}$ is proportional to the unit matrix. The outgoing density is given by $\tilde{\rho}_j = \Psi^\dagger S^\dagger \rho_j S\Psi$ or in terms of the density matrix $\tilde{\rho}_j = S^\dagger \rho_j S$. We can now implement this in the formula we obtained for the linear conductance. This gives us the following relation:

$$G_{jk} = \delta_{jk} - Tr[\rho_{j,out}\rho_{j,in}] = \delta_{jk} - Tr[\tilde{\rho}_j\rho_j] \tag{33}$$

We wish to reduce the redundancies of our conductance matrix and therefore define, consistent with the current conservation laws $\sum_j G_{jk} = 0$ and $\sum_k G_{jk} = 0$, certain combinations of voltages. We define $(I_a, I_b, I_0) = \tilde{G}(V_a, V_b, V_0)$ with

$$
\begin{aligned}
V_a &= (V_1 - V_2), & I_a &= (I_1 - I_2), \\
V_b &= (V_1 + V_2 - 2V_3)/2, & I_b &= (I_1 + I_2 - 2I_3), \\
V_0 &= (V_1 + V_2 + V_3)/3, & I_0 &= (I_1 + I_2 + I_3).
\end{aligned}
\tag{34}
$$

The connection between $\tilde{G}$ and G is given by $\tilde{G} = AR^\dagger GRA$ with $A = diag(\frac{1}{\sqrt{2}}, \sqrt{\frac{2}{3}}, \sqrt{3})$ and

$$
R = \begin{pmatrix}
\frac{1}{\sqrt{2}} & \frac{1}{\sqrt{6}} & \frac{1}{\sqrt{3}} \\
-\frac{1}{\sqrt{2}} & \frac{1}{\sqrt{6}} & \frac{1}{\sqrt{3}} \\
0 & \frac{-2}{\sqrt{6}} & \frac{1}{\sqrt{3}}
\end{pmatrix},
\tag{35}
$$

such that $R^\dagger R = \mathbb{1}$. We obtain

$$
\tilde{G} = \begin{pmatrix}
\frac{1}{4}(G_{11} - G_{21} + G_{22} - G_{12}) & \dots \\
\frac{1}{6}(G_{11} + G_{21} - 2G_{31} - G_{12} - G_{22} + 2G_{32}) & \dots \\
0 & \dots
\end{pmatrix}
$$

$$
\begin{pmatrix}
\dots & \frac{1}{6}(G_{11} - G_{21} + G_{22} - G_{12} - G_{13} + G_{23}) & 0 \\
\dots & \frac{1}{9}((G_{11} + G_{21} - 2G_{31} + G_{12} + G_{22} - 2G_{32} - 2(G_{13} + G_{23} - 2G_{33})) & 0 \\
\dots & 0 & 0
\end{pmatrix}.
\tag{36}
$$

The third row and column are equal to zero, because of charge conservation and because applying equal voltages will not produce a current. The remaining components are nonzero. We obtain the reduced 2x2 conductance Matrix, which takes the form:

$$\tilde{G} = \begin{pmatrix} \frac{1}{2}(1 - \frac{1}{2}Tr(\tilde{\lambda}_3\lambda_3)) & -\frac{1}{2\sqrt{3}}Tr(\tilde{\lambda}_3\lambda_8) & 0 \\ -\frac{1}{2\sqrt{3}}Tr(\tilde{\lambda}_8\lambda_3) & \frac{1}{2}(1 - \frac{2}{3}Tr(\tilde{\lambda}_8\lambda_8)) & 0 \\ 0 & 0 & 0 \end{pmatrix}, \qquad (37)$$

with $\tilde{\lambda}_i = S^\dagger\lambda_i S$. The general S-matrix contains eight Euler angles, however, the conductance includes only traces of products of $\lambda_{3(8)}$ and $S^\dagger\lambda_{3(8)}S$. Since λ_3 and λ_8 commute with each other, the angles $\alpha_4, \alpha_3, \alpha_2$ drop out of any observable quantity. One can also redefine the angles in such way, that ϕ' can be set to zero. [23]. Our result is a S-matrix which can be parameterized by four angles:

$$S = e^{i\lambda_2\frac{\chi}{2}}e^{i\lambda_3\frac{(\pi-\Psi)}{2}}e^{i\lambda_5\theta}e^{i\lambda_2\frac{\chi'}{2}}. \qquad (38)$$

or equivalently

$$S = \begin{pmatrix} e^{i\frac{\pi-\Psi}{2}}\cos(\theta)\cos\left(\frac{\chi}{2}\right)\cos\left(\frac{\chi'}{2}\right) - e^{-i\frac{\pi-\Psi}{2}}\sin\left(\frac{\chi}{2}\right)\sin\left(\frac{\chi'}{2}\right) & \dots \\ -e^{i\frac{\pi-\Psi}{2}}\cos(\theta)\sin\left(\frac{\chi}{2}\right)\cos\left(\frac{\chi'}{2}\right) - e^{-i\frac{\pi-\Psi}{2}}\cos\left(\frac{\chi}{2}\right)\sin\left(\frac{\chi'}{2}\right) & \dots \\ -\sin(\theta)\cos\left(\frac{\chi'}{2}\right) & \dots \end{pmatrix}$$

$$\begin{pmatrix} \dots & e^{i\frac{\pi-\Psi}{2}}\cos(\theta)\cos\left(\frac{\chi}{2}\right)\sin\left(\frac{\chi'}{2}\right) + e^{-i\frac{\pi-\Psi}{2}}\sin\left(\frac{\chi}{2}\right)\cos\left(\frac{\chi'}{2}\right) & e^{i\frac{\pi-\psi}{2}}\sin(\theta)\cos\left(\frac{\chi}{2}\right) \\ \dots & -e^{i\frac{\pi-\Psi}{2}}\cos(\theta)\sin\left(\frac{\chi}{2}\right)\sin\left(\frac{\chi'}{2}\right) + e^{-i\frac{\pi-\Psi}{2}}\cos\left(\frac{\chi}{2}\right)\cos\left(\frac{\chi'}{2}\right) & -e^{i\frac{\pi-\psi}{2}}\sin(\theta)\sin\left(\frac{\chi}{2}\right) \\ \dots & -\sin(\theta)\sin\left(\frac{\chi'}{2}\right) & \cos(\theta) \end{pmatrix} \qquad (39)$$

We now want to integrate the helical transport in the S-matrix, as much as the unitary condition allows it. We want to set $r_{33} = 0$ to 0, since we do not allow backscattering in the same channel. Therefore we choose $\theta = \frac{\pi}{2}$.

$$S = \begin{pmatrix} -e^{-i\frac{\pi-\Psi}{2}}\sin\left(\frac{\chi}{2}\right)\sin\left(\frac{\chi'}{2}\right) & e^{-i\frac{\pi-\Psi}{2}}\sin\left(\frac{\chi}{2}\right)\cos\left(\frac{\chi'}{2}\right) & e^{i\frac{\pi-\psi}{2}}\cos\left(\frac{\chi}{2}\right) \\ -e^{-i\frac{\pi-\Psi}{2}}\cos\left(\frac{\chi}{2}\right)\sin\left(\frac{\chi'}{2}\right) & e^{-i\frac{\pi-\Psi}{2}}\cos\left(\frac{\chi}{2}\right)\cos\left(\frac{\chi'}{2}\right) & -e^{i\frac{\pi-\psi}{2}} \\ -\cos\frac{\chi'}{2}) & -\sin\left(\frac{\chi'}{2}\right) & 0 \end{pmatrix}. \qquad (40)$$

In a next step we would like to eliminate $r_{22} = 0$ and therefore choose $\chi = \pi$

$$S = \begin{pmatrix} -e^{-i\frac{\pi-\Psi}{2}}\sin\left(\frac{\chi'}{2}\right) & e^{-i\frac{\pi-\Psi}{2}}\cos\left(\frac{\chi'}{2}\right) & 0 \\ 0 & 0 & -e^{i\frac{\pi-\psi}{2}} \\ -\cos\frac{\chi'}{2}) & -\sin\left(\frac{\chi'}{2}\right) & 0 \end{pmatrix}. \qquad (41)$$

In the last step we can eliminate $r_{11} = 0$, $\chi' = 0$ and get

$$S = \begin{pmatrix} 0 & e^{-i\frac{\pi-\Psi}{2}} & 0 \\ 0 & 0 & -e^{i\frac{\pi-\psi}{2}} \\ -1 & 0 & 0 \end{pmatrix}. \qquad (42)$$

If all reflection coefficients are set to zero, there is a trivial solution, where single channels are connected with perfect transmission (Figure 11).
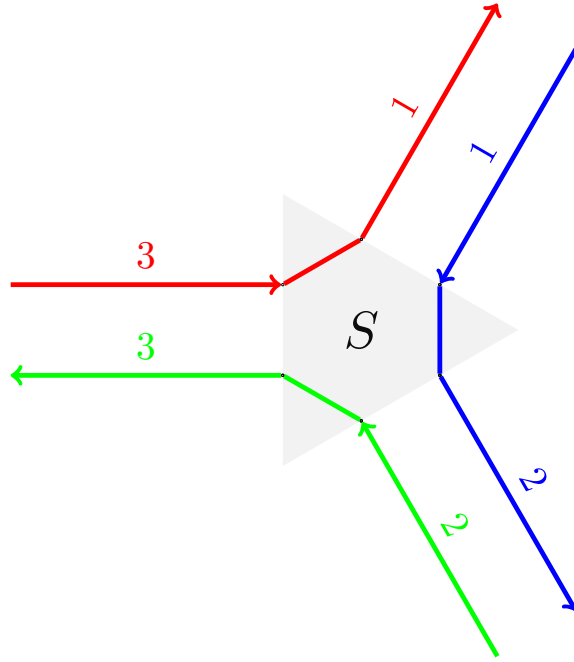

Figure 11: The S-Matrix connects single channels with perfect transmission.

C   Transmission coefficient in Section 3.2

From the following Eqs.(43) we can compute the transmission coefficient in Section 3.2.

$$\begin{pmatrix} m \\ h \end{pmatrix}_{out,left} = S_L \begin{pmatrix} m \\ h \end{pmatrix}_{in,left} \,, \quad \begin{pmatrix} e^{-i\frac{\lambda}{2}}\Phi^\dagger h_{l,in} \\ m_{r,out} \end{pmatrix} = S_R \begin{pmatrix} e^{i\frac{\lambda}{2}}\Phi h_{l,out} \\ m_{r,in} \end{pmatrix}, \quad (43)$$

$$h_{l,out} = t_L m_{l,in} + r'_L h_{l,in}, \tag{44}$$

$$e^{-i\frac{\lambda}{2}}\Phi^\dagger h_{l,in} = r_R e^{i\frac{\lambda}{2}}\Phi h_{l,out} + t'_R m_{r,in}. \tag{45}$$

Let us insert Eq.(44) in Eq.(45). This yields

$$e^{-i\frac{\lambda}{2}}\Phi^\dagger h_{l,in} = r_R e^{i\frac{\lambda}{2}}\Phi(t_L m_{l,in} + r'_L h_{l,in}) + t'_R m_{r,in}, \tag{45a}$$

$$e^{-i\frac{\lambda}{2}}\Phi^\dagger h_{l,in} - r_R e^{i\frac{\lambda}{2}}\Phi r'_L h_{l,in} = r_R e^{i\frac{\lambda}{2}}\Phi t_L m_{l,in} + t'_R m_{r,in}, \tag{45b}$$

$$h_{l,in} - e^{i\lambda}\Phi r_R \Phi r'_L h_{l,in} = \Phi r_R e^{i\lambda}\Phi t_L m_{l,in} + e^{i\frac{\lambda}{2}}\Phi t'_R m_{r,in}, \tag{45c}$$

$$h_{l,in} = [\mathbb{1} - e^{i\lambda}\Phi r_R \Phi r'_L]^{-1}\left(\Phi r_R e^{i\lambda}\Phi t_L m_{l,in} + e^{i\frac{\lambda}{2}}\Phi t'_R m_{r,in}\right). \tag{45d}$$

Eliminating $h_{l,in}$ in Eq.(44) gives

$$h_{l,in} = [\mathbb{1} - \Phi r_R \Phi r'_L]^{-1}\left(\Phi r_R e^{i\lambda}\Phi t_L m_{l,in} + e^{i\frac{\lambda}{2}}\Phi t'_R m_{r,in}\right),$$
$$h_{l,out} = t_L m_{l,in} + r'_L \left([\mathbb{1} - \Phi r_R \Phi r'_L]^{-1}\left(\Phi r_R e^{i\lambda}\Phi t_L m_{l,in} + e^{i\frac{\lambda}{2}}\Phi t'_R m_{r,in}\right)\right). \tag{46}$$

We can compare the definition of $m_{l,out}$ we get from the S-Matrix:

$$m_{l,out} = r m_{l,in} + t' m_{r,in}, \tag{47}$$

and from the S-matrix at the junction:

$$m_{l,out} = r_L m_{l,in} + t'_L h_{l,in}. \tag{48}$$

We now insert $h_{l,in}$ in Eq.(48) and compare the expressions Eq.(47) and Eq.(48). This gives us

$$t' = t'_L[\mathbb{1} - e^{i\lambda}\Phi r_R \Phi r'_L]^{-1}\Phi e^{i\frac{\lambda}{2}}t'_R, \tag{49}$$

$$t = t_R[\mathbb{1} - e^{i\lambda}\Phi r'_L \Phi r_R]^{-1}\Phi e^{i\frac{\lambda}{2}}t_L. \tag{50}$$

D Explicit calculation on the conductance in Section 3.2

The Landauer formula can be evaluated using Eq.(18)

$$
G = \frac{e^2}{h} Tr[t^\dagger t]
$$

$$
= \frac{e^2}{h} Tr \left[\left(t_R[\mathbb{1} - e^{i\lambda}\Phi r'_L \Phi r_R]^{-1} \Phi e^{i\frac{\lambda}{2}} t_L \right)^\dagger \left(t_R[\mathbb{1} - e^{i\lambda}\Phi r'_L \Phi r_R]^{-1} \Phi e^{i\frac{\lambda}{2}} t_L \right) \right]
$$

$$
= \frac{e^2}{h} Tr \left[t_R t_R^\dagger t_L t_L^\dagger \left([\mathbb{1} - e^{i\lambda}\Phi r'_L \Phi r_R]^{-1} \right)^\dagger [\mathbb{1} - e^{i\lambda}\Phi r'_L \Phi r_R]^{-1} \right]. \quad (51)
$$

For the inverted Matrix in equation 51 we get

$$
\left[\mathbb{1} - e^{i\lambda} \begin{pmatrix} e^{-i\varphi/2} & 0 \\ 0 & e^{i\varphi/2} \end{pmatrix} \begin{pmatrix} r_L^* & 0 \\ 0 & r_L^* \end{pmatrix} \begin{pmatrix} e^{-i\varphi/2} & 0 \\ 0 & e^{i\varphi/2} \end{pmatrix} \begin{pmatrix} r_R & 0 \\ 0 & r_R \end{pmatrix} \right]^{-1} \quad (52)
$$

$$
= \left[\mathbb{1} - e^{i\lambda} \begin{pmatrix} e^{-i\varphi} r_R r_L^* & 0 \\ 0 & e^{i\varphi} r_R r_L^* \end{pmatrix} \right]^{-1} \quad (53)
$$

$$
= \left[\begin{pmatrix} 1 - e^{i\lambda} e^{-i\varphi} r_R r_L^* & 0 \\ 0 & 1 - e^{i\lambda} e^{i\varphi} r_R r_L^* \end{pmatrix} \right]^{-1} \quad (54)
$$

$$
= \begin{pmatrix} \frac{1}{1 - e^{i\lambda} e^{-i\varphi} r_R r_L^*} & 0 \\ 0 & \frac{1}{1 - e^{i\lambda} e^{i\varphi} r_R r_L^*} \end{pmatrix}. \quad (55)
$$

For $\left([\mathbb{1} - e^{i\lambda}\Phi r'_L \Phi r_R]^{-1} \right)^\dagger [\mathbb{1} - e^{i\lambda}\Phi r'_L \Phi r_R]^{-1}$ we get

$$
\begin{pmatrix} \frac{1}{1 - e^{i\lambda} e^{-i\varphi} r_R r_L^*} & 0 \\ 0 & \frac{1}{1 - e^{i\lambda} e^{i\varphi} r_R r_L^*} \end{pmatrix}^\dagger \begin{pmatrix} \frac{1}{1 - e^{i\lambda} e^{-i\varphi} r_R r_L^*} & 0 \\ 0 & \frac{1}{1 - e^{i\lambda} e^{i\varphi} r_R r_L^*} \end{pmatrix} \quad (56)
$$

$$
= \begin{pmatrix} \frac{1}{1 - e^{i(\lambda-\varphi)} r_R r_L^* - e^{-i(\lambda-\varphi)} r_R^* r_L + |r_R|^2 |r_L|^2} & 0 \\ 0 & \frac{1}{1 - e^{i(\lambda+\varphi)} r_R r_L - e^{-i(\lambda+\varphi)} r_R^* r_L + |r_R|^2 |r_L|^2} \end{pmatrix}.
$$

$$
(57)
$$

E   Explicit calculation of $S = -QS^TQ$ in Section 3.2

If our setup has TRS the S-Matrix satisfies the following relation [19, 20]:

$$S\Psi_{in} = -QS^TQ\Psi_{in} \tag{58}$$

$$= -QT^{-1}UKS^TKU^{-1}TQ\Psi_{in} \tag{59}$$

$$= -QT^{-1}US^\dagger U^{-1}TQ\Psi_{in} \tag{60}$$

$$= -QT^{-1}US^\dagger U^{-1}T^2\Psi_{out} \tag{61}$$

$$= QT^{-1}US^\dagger U^{-1}\Psi_{out} \tag{62}$$

$$= QT^{-1}\Psi_{in} \tag{63}$$

$$= Q^2TQ\Psi_{in} = \Psi_{out} = S\Psi_{in}, \tag{64}$$

where we used that $T^2 = -\mathbb{1}$ for fermions, which gives the relation above.

Eigenständigkeitserklärung

Hiermit erkläre ich, die vorliegende Arbeit selbständig verfasst zu haben und keine anderen als die in der Arbeit angegebenen Quellen und Hilfsmittel benutzt zu haben.
München, 28. Juni 2017
Unterschrift